Generation of Greenberger-Horne-Zeilinger States on Two-Dimensional Superconducting-Qubit Lattices via Parallel Multiqubit-Gate Operations

Wei Feng,[1] Guo-Qiang Zhang,[1] Qi-Ping Su,[1] Jun-Xiang Zhang,[2,*] and Chui-Ping Yang[1,3,†]

[1] *School of Physics, Hangzhou Normal University, Hangzhou 311121, China*
[2] *School of Physics, Zhejiang University, Hangzhou 310027, China*
[3] *Quantum Information Research Center, Shangrao Normal University, Shangrao 334001, China*

(Received 17 June 2022; accepted 21 November 2022; published 13 December 2022)

A recent major technological breakthrough in superconducting circuits is the realization of more than 50 qubits arranged on two-dimensional (2D) lattices with tunable nearest-neighbor couplings. We propose a protocol to generate Greenberger-Horne-Zeilinger (GHZ) states on 2D superconducting-qubit lattices by applying multiqubit controlled-*i*SWAP gates in parallel. The multiqubit gate can be naturally implemented based on an effective three-body interaction, which can be synthesized with appropriate detunings and coupling strengths between qubits. We simulate the preparation process of GHZ states with realistic parameters, and show a 37-qubit GHZ state can be generated with a controlled-*i*SWAP depth of 3. Our proposal provides a more promising method of generating GHZ states on the latest 2D superconducting-qubit architectures and will stimulate the preparation of multiqubit entangled states based on multiqubit gates.

DOI: 10.1103/PhysRevApplied.18.064036

I. INTRODUCTION

The generation of entanglement across a device is a technical milestone on the road to scale up quantum processors and demonstrate quantum advantage. In addition to testing fundamental quantum theories [1–3], entangled states play an essential role in quantum computation [4], quantum information [5], and quantum-enhanced measurements [6]. In particular, Greenberger-Horne-Zeilinger (GHZ) states [7], the maximally entangled states of three or more particles, were proposed to verify Bell's inequality, and later were found useful in quantum metrology [8], quantum cryptography [9], etc. Much effort has been devoted to generating GHZ states in different quantum systems, including photonic [10–13], cavity QED [14, 15], ion trap [16–18], Bose-Einstein-condensed [19,20], nitrogen-vacancy (N-V) center [21], optomechanical [22], and quantum dot [23] systems.

Superconducting circuits, which have advantages in tunability, flexibility, and scalability with solid-state microfabrication technology, are a rapidly developing platform for quantum computation [24–27]. Moreover, in contrast to natural atoms, superconducting qubits can have strong coupling with microwave resonators and can be designed with special characteristics. These merits have made superconducting circuits ideal for studying many quantum optics phenomenons that are difficult to achieve with natural atoms [28,29]. In recent years, a lot of breakthroughs in key technologies have been made with superconducting circuits, especially in tunable qubit-qubit coupling [30–33] and two-dimensional (2D) architecture [34–39]. These technological breakthroughs have led to several significant experiments, such as the demonstration of quantum supremacy (advantage) [35,37], 2D quantum walks [36], and quantum adversarial learning [39].

Many theoretical schemes have been proposed for generating GHZ states in superconducting circuits [40–49]. In experiments previously reported, two main methods were used for preparing GHZ states of superconducting qubits. One method is based on sequential CNOT gates [50–53], and an 18-qubit GHZ state with a fidelity of 0.5165 was achieved [53]. The CNOT depth required to generate a N-qubit GHZ state scales as $O(N)$ even using the gates in parallel. Limited by qubit decoherence, a GHZ state involving more qubits is hard to generate. The other method relies on a fully connected architecture where all qubits couple to a common resonator [54,55]. The resonator-induced qubit-qubit collective interaction can, in principle, one-step entangle all qubits into a GHZ state from an initial product state. Using this method, an 18-qubit GHZ state was also achieved with a fidelity of 0.525 [55]. The second method is efficient but it requires all the qubit-qubit effective coupling strengths to be the same. In practical, the inhomogeneity of the qubit-resonator couplings and the crosstalk between neighboring qubits drop the fidelity of GHZ states, which becomes more significant

*junxiang_zhang@zju.edu.cn
†yangcp@hznu.edu.cn

as the number of qubits is increased. For the latest 2D superconducting qubit architectures without a common resonator [35–37], an alternative scheme is highly needed to generate multiqubit GHZ states.

In this paper, we give a promising mechanism to efficiently generate GHZ states on the 2D superconducting-qubit lattices previously reported. The method is based on a multiqubit controlled-*i*SWAP gate, which can be naturally implemented from an effective three-body interaction [56]. With a controlled-*i*SWAP depth of 3, we can obtain a 37-qubit GHZ state. In contrast, the 18-qubit GHZ state was generated with a CNOT depth of 6 in Ref. [53]. We also numerically simulate the preparation process based on the original Hamiltonians of lattices. With a group of realistic parameters, the fidelity of the 37-qubit GHZ state is larger than 0.5, which confirms our method is feasible with existing superconducting-qubit lattices.

This paper is organized as follows: In Sec. II, we introduce the model and the method for generating effective three-body interactions in superconducting-qubit lattices. In Sec. III, we present the scheme for implementing the multiqubit controlled-*i*SWAP gate based on the three-body interaction. In Sec. IV, we describe the protocol for generating GHZ states using the multitarget-qubit controlled-*i*SWAP gate and discuss the experimental feasibility with numerical simulation. Finally, we make a conclusion in Sec. V.

II. MODEL AND EFFECTIVE HAMILTONIAN

We consider two types of experimentally achievable 2D superconducting qubit lattices: triangular [34] and rectangular lattices [35–39], as shown in Figs. 1(a) and 1(b), respectively. The resonant frequencies of qubits and the coupling strengths between nearest-neighbor qubits are both tunable. Firstly, we look at the triangular lattice and focus on the central qubit (Q_0) and its six nearest-neighbor qubits (Q_j for $j = 1-6$). The couplings between Q_j and its peripheral qubits can be turned off, and the Hamiltonian of the subsystem is (setting $\hbar = 1$)

$$H = \omega_0 \left|1_0\right\rangle\left\langle 1_0\right| + \sum_{j=1}^{6}\Big[\omega_j \left|1_j\right\rangle\left\langle 1_j\right| + g_j\left(\sigma_j^+\sigma_0^- + \sigma_j^-\sigma_0^+\right) + g_{j(j+1)}\left(\sigma_j^+\sigma_{j+1}^- + \sigma_j^-\sigma_{j+1}^+\right)\Big], \tag{1}$$

where $\sigma_j^+(\sigma_j^-)$ is the raising (lowering) operator with $\left|0_j\right\rangle$ ($\left|1_j\right\rangle$) being the ground (excited) state of Q_j, ω_j is the resonant frequency of Q_j, g_j is the coupling strength between Q_j and Q_0, and $g_{j(j+1)}$ is the coupling strength between Q_j and Q_{j+1} with j running cyclically from 1 to 6.

Besides the original coupling $g_{j(j+1)}$, Q_j and Q_{j+1} can have an additional second-order coupling mediated by the central qubit Q_0. If we detune all Q_j ($j = 1-6$) from Q_0 by the same amount Δ and $|\Delta| \gg g_j$, then there will be an all-to-all superexchange (SE) interaction [57], i.e., any two of the qubits Q_j and Q_k will have a second-order coupling mediated by Q_0. We can also use multiplexing to turn on intrapair SE interactions simultaneously by arranging multiple qubit pairs at different detunings. Without loss of generality, we divide the six qubits Q_j into three pairs: $Q_1 - Q_2$, $Q_3 - Q_4$, and $Q_5 - Q_6$, and detune them from Q_0 by Δ_j ($\equiv \omega_j - \omega_0$, and $\omega_j = \omega_{j+1}$) for $j = 1$, 3, and 5, respectively. Further, we focus on the three-qubit unit cell of $Q_0 - Q_1 - Q_2$. When the central qubit Q_0 is initially in

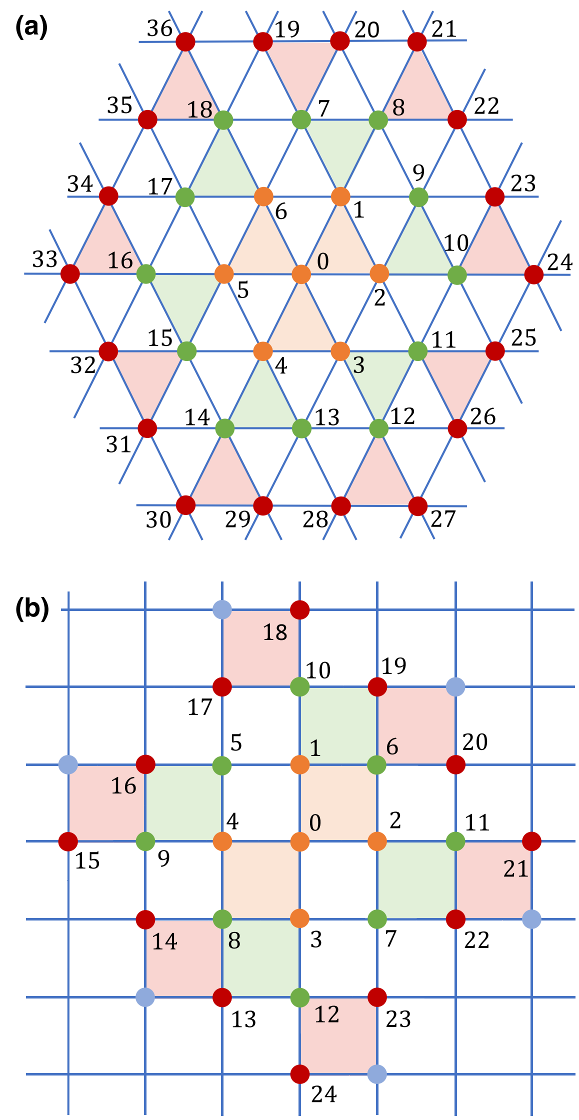

FIG. 1. Schematic of 2D superconducting-qubit lattices. The dots labeled with numbers represent the qubits arranged in (a) triangular and (b) rectangular lattices. Each qubit couples to its nearest neighbors, and the coupling strengths and the resonant frequencies of the qubits are both tunable. The highlighted triangles and rectangles represent the multiqubit gate operations on the related qubits.

the ground state, the states $|0_0 1_1 0_2\rangle$ and $|0_0 0_1 1_2\rangle$ can have a second-order coupling mediated by $|1_0 0_1 0_2\rangle$, and the effective coupling strength is $g_1 g_2/\Delta_1$. When the central qubit Q_0 is initially in the excited state, the states $|1_0 1_1 0_2\rangle$ and $|1_0 0_1 1_2\rangle$ can have a second-order coupling mediated by $|0_0 1_1 1_2\rangle$, and the effective coupling strength is $-g_1 g_2/\Delta_1$. Note that the above two effective coupling strengths have opposite signs. This is because the intermediate state $|1_0 0_1 0_2\rangle$ has a lower (higher) energy than the initial states $|0_0 1_1 0_2\rangle$ and $|0_0 0_1 1_2\rangle$ while the intermediate state $|0_0 1_1 1_2\rangle$ has a higher (lower) energy than the initial states $|1_0 1_1 0_2\rangle$ and $|1_0 0_1 1_2\rangle$, with the detuning Δ_1 being positive (negative). The feature that the second-order coupling depends on the state of intermediary qubit can be expressed as a three-body interaction $\sigma_0^z\left(\sigma_1^+\sigma_2^- + \sigma_1^-\sigma_2^+\right)$ with a coefficient $g_1 g_2/\Delta_1$, where $\sigma_0^z = |0_0\rangle\langle 0_0| - |1_0\rangle\langle 1_0|$ is the Pauli operator. On the whole, the effective Hamiltonian under a second-order perturbation is

$$H_{\rm eff} = \sum_{j=1,3,5}\left(\lambda_j\sigma_0^z + g_{j(j+1)}I_0\right)\left(\sigma_j^+\sigma_{j+1}^- + \sigma_j^-\sigma_{j+1}^+\right) + \sum_{j=1}^{6}\frac{g_j^2}{\Delta_j}\left(|1_j\rangle\langle 1_j| - |1_0\rangle\langle 1_0|\right), \quad (2)$$

where I_0 is the identity operator of Q_0, $\lambda_j = g_j g_{j+1}/\Delta_j$, $|\Delta_j| \gg g_j, g_{j+1}$, and $|\Delta_j - \Delta_k| \gg \lambda_j, \lambda_k$ for $j,k \in \{1,3,5\}$. With this setting, the interpair couplings are effectively turned off due to large detunings between different pairs, and the three intrapair second-order couplings mediated by the central qubit Q_0 are simultaneously generated. For the rectangular lattice shown in Fig. 1(b), parallel intrapair SE interactions for $Q_1 - Q_2$, and $Q_3 - Q_4$ can also be constructed in the same way.

III. IMPLEMENTATION OF MULTIQUBIT CONTROLLED-*i*SWAP GATE

From the effective Hamiltonian in Eq. (2), we see that the intrapair couplings for each pair of qubits have two components: the direct coupling (with strength $g_{j(j+1)}$) and the second-order coupling (with strength λ_j) mediated by Q_0. Both of these coupling strengths are tunable. If we set $\lambda_j = -g_{j(j+1)}$, the two coupling components cancel each other when Q_0 is in the ground state and sum up when Q_0 is in the excited state. Thus the central qubit Q_0 can serve as a controller to turn on and off the multiple intrapair couplings simultaneously. We simulate this kind of parallel multiqubit controlled-swapping dynamics using the original Hamiltonian H with experimentally feasible parameters of superconducting qubit lattices [37], and the results are shown in Fig. 2. One can see that, the excitations of Q_j ($j = 1,3,5$) are almost unchanged when Q_0 is in the ground state, except the leakages to the environments and

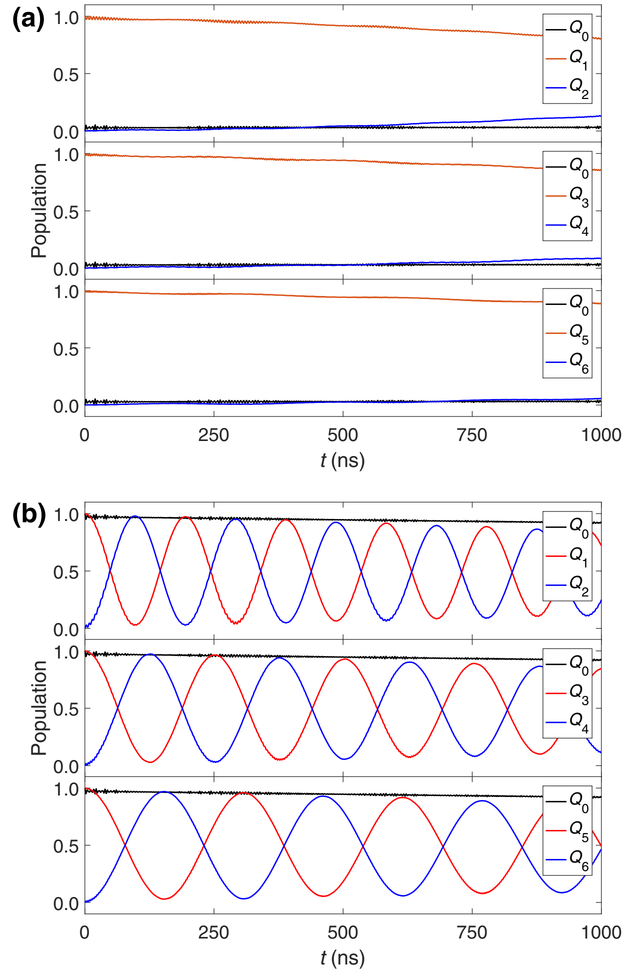

FIG. 2. Parallel multiqubit controlled-swapping dynamics. Time evolution of populations of Q_j is simulated using the original Hamiltonian H with initial state (a) $|0_0 1_1 0_2 1_3 0_4 1_5 0_6\rangle$ and (b) $|1_0 1_1 0_2 1_3 0_4 1_5 0_6\rangle$. Relevant parameters are chosen as $g_j = 15$ MHz for $j = 1-6$, $\Delta_1 = -170$ MHz, $\Delta_3 = -220$ MHz, $\Delta_5 = -270$ MHz, $g_{j(j+1)} = -\lambda_j = -g_j g_{j+1}/\Delta_j$ for $j = 1,3,5$, and the relaxation and pure dephasing times of the superconducting qubits are $T_1 = 20\ \mu$s and $T_2^* = 5\ \mu$s, respectively.

paired qubits due to the dissipations and higher-order coupling, respectively. The tiny high-frequency oscillations in the simulated curves are due to the off-resonant transitions with large detunings. When Q_0 is in the excited state, the parallel intrapair Rabi oscillations with different frequencies for $Q_1 - Q_2$, $Q_3 - Q_4$, and $Q_5 - Q_6$ are clearly observed in Fig. 2(b).

Further, the oscillation frequencies $|2\lambda_j|$ of the three-qubit pairs can be changed to the same value by adjusting g_j. For example, if we set $g_1 = g_2$, $g_3 = g_4 = \sqrt{\Delta_3/\Delta_1}g_1$, and $g_5 = g_6 = \sqrt{\Delta_5/\Delta_1}g_1$, then $\lambda_j = \lambda = g_1^2/\Delta_1$ for $j = 1,3,5$, and the three-qubit pairs will have the same gate time $t_{i\rm SWAP} = |\pi/4\lambda|$ to complete the population swapping when Q_0 is in the excited state. Based on the above dynamics, we can naturally obtain a multiqubit controlled-iSWAP gate, which is described by

$$U_{\mathrm{MCS},n} = |0\rangle\langle 0| \otimes I^{\otimes 2n} + |1\rangle\langle 1| \otimes [U_{i\mathrm{SWAP}}]^{\otimes n}, \quad (3)$$

where MCS is the abbreviation for multiqubit controlled iSWAP, n is the number of target-qubit pairs, and

$$U_{i\mathrm{SWAP}} = \begin{bmatrix} 1 & 0 & 0 & 0 \\ 0 & 0 & -i & 0 \\ 0 & -i & 0 & 0 \\ 0 & 0 & 0 & 1 \end{bmatrix} \quad (4)$$

is the usual two-qubit iSWAP gate. The $U_{\mathrm{MCS},3}$ of the seven-qubit subsystem can result in the typical state transitions

$$\begin{aligned} U_{\mathrm{MCS},3}|0101010\rangle &= |0101010\rangle, \\ U_{\mathrm{MCS},3}|1101010\rangle &= i|1010101\rangle, \end{aligned} \quad (5)$$

where the subscripts of the qubit index are omitted for clarity. A three-qubit gate $U_{\mathrm{MCS},1}$ or five-qubit gate $U_{\mathrm{MCS},2}$ acting on selected qubits can be flexibly realized in a similar way, and a multiqubit gate $U_{\mathrm{MCS},n}$ involving more qubits can be implemented if the central qubit connects with additional qubits.

For the rectangular lattice shown in Fig. 1(b), the multiqubit controlled-iSWAP gate can also be implemented with the help of auxiliary qubit. For qubit pair $Q_1 - Q_2$ in the rectangular lattice, besides the second-order coupling mediated by Q_0, another equal-strength second-order couplings mediated by auxiliary qubit Q_6 can be realized with suitable detunings. If we keep Q_6 in the ground state, then these two second-order couplings will cancel each other when Q_0 is in the excited state and sum up when Q_0 is in the ground state. Therefore, the construction method of the multiqubit gate on the triangular lattice can be easily extended to the rectangular lattice.

IV. PREPARATION OF GHZ STATES

In this section, we demonstrate the protocol for generating GHZ states based on the multiqubit controlled-iSWAP gates. As the preparation circuits shown in Fig. 3 for the triangular lattice, a 37-qubit GHZ state can be generated with three steps:

(1) Starting from the system's ground state $|00\cdots 0\rangle$, apply a Hadamard gate on Q_0 and a Pauli-X gate on one qubit of each pair, prepare the subsystem in the state $1/\sqrt{2}\,(|0\rangle + |1\rangle) \otimes |101010\rangle$. Then apply the seven-qubit controlled-iSWAP gate $U_{\mathrm{MCS},3}$ followed by Pauli-X gates, this brings the subsystem into a seven-qubit GHZ state $|\Psi_1\rangle = 1/\sqrt{2}\left(|0\rangle^{\otimes 7} + e^{i\varphi_1}|1\rangle^{\otimes 7}\right)$, where φ_1 may not be equal to $\pi/2$ as in Eq. (5) due to the energy shifts in Eq. (2), and this phase does not affect entanglement.

(2) Apply six three-qubit controlled-iSWAP gates in parallel from Q_{1-6} to their outer qubit pairs, with flipping one qubit of each pair before and after. The GHZ state can be extended to $|\Psi_2\rangle = 1/\sqrt{2}\left(|0\rangle^{\otimes 19} + e^{i\varphi_2}|1\rangle^{\otimes 19}\right)$.

(3) Repeat the above operation by applying three-qubit controlled-iSWAP gates in parallel from qubits that are already included in the growing GHZ state. After the controlled-iSWAP operations with a depth of 3, the 37 qubit shown in Fig. 1(a) can all be entangled in the GHZ state $|\Psi_3\rangle = 1/\sqrt{2}\left(|0\rangle^{\otimes 37} + e^{i\varphi_3}|1\rangle^{\otimes 37}\right)$.

The GHZ state can be further extended if the lattice epitaxy has more qubits, and the total number of qubits in the GHZ state scales $3n^2 + 3n + 1$ where n is the depth of the multiqubit gate operations. For the rectangular lattice, GHZ states can be generated in a similar way. Within a controlled-iSWAP depth of 1, 2, and 3, the numbers of entangled qubits in the GHZ states are 5, 13, and 25, respectively, as shown in Fig. 1(b).

We simulate the preparation process in step 1 based on the Lindblad master equation with the original Hamiltonian and experimentally feasible parameters. The simulated seven-qubit and five-qubit GHZ density matrices ρ_{sim} with sim being the abbreviation for simulation are shown in Figs. 4(a) and 4(b), respectively. The fidelities $\mathrm{Tr}\left(\rho_{\mathrm{ideal}}\rho_{\mathrm{sim}}\right)$ relating to the ideal GHZ state $|\Psi_1\rangle = 1/\sqrt{2}\left(|0\rangle^{\otimes N} + e^{i\varphi_1}|1\rangle^{\otimes N}\right)$ for triangular ($N = 7$) and rectangular ($N = 5$) lattices are $F_{\mathrm{tri}}^{(1)} = 0.920$ and $F_{\mathrm{rec}}^{(1)} = 0.927$, respectively. We also simulate the case that just one

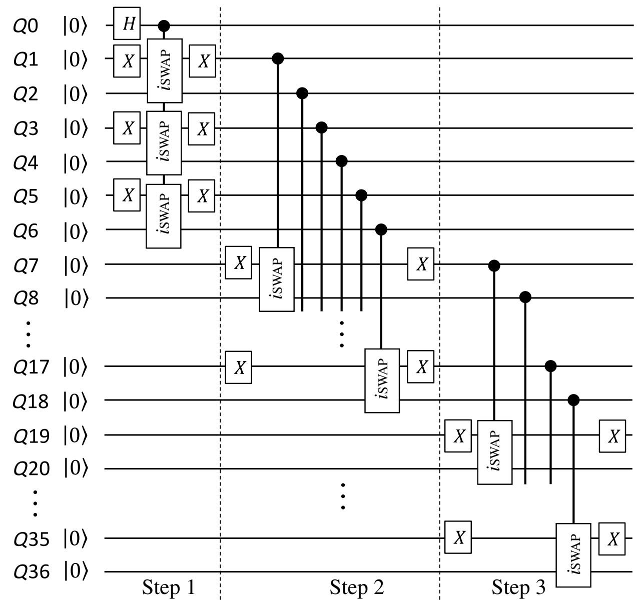

FIG. 3. Quantum circuit for generating GHZ states with parallel multiqubit controlled-iSWAP gates. The preparation circuit is suited for the triangular qubit lattice shown in Fig. 1(a). In step 1, a seven-qubit controlled-iSWAP gate is used to one-step generate a seven-qubit GHZ state. In step 2 (3), six (nine) three-qubit controlled-iSWAP gates can be applied in parallel from qubits that are already included in the growing GHZ state. Within a controlled-iSWAP depth of 3, we can obtain a 37-qubit GHZ state.

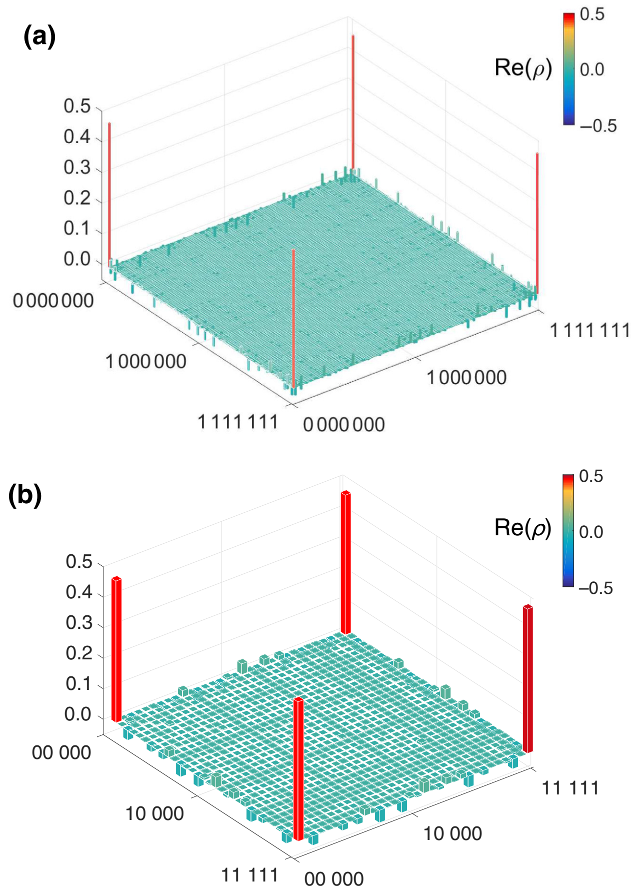

FIG. 4. Density matrices of entangled subsystems after first step of the GHZ state preparation for (a) triangular and (b) rectangular lattices, with fidelities of $F_{\mathrm{tri}}^{(1)} = 0.920$, and $F_{\mathrm{rec}}^{(1)} = 0.927$, respectively. For clarity of display, here a single-qubit z-axis rotation by an angle of φ_1 is numerically applied to Q_1 to cancel the arguments of the major off-diagonal elements. The simulations are based on the Lindblad master equation. For the triangular lattice in (a), the original Hamiltonian is used with the same parameters as in Fig. 2 except $g_{1,2} = 15$ MHz, $g_{3,4} = \sqrt{\Delta_3/\Delta_1}g_1$, and $g_{5,6} = \sqrt{\Delta_5/\Delta_1}g_1$. In (b), an analogous Hamiltonian and the same parameters are used for the rectangular lattice.

pair of qubits is in work, where the three-qubit gate $U_{\mathrm{MCS},1}$ induce three-qubit GHZ states with fidelities $F_{\mathrm{tri},3} = 0.983$ and $F_{\mathrm{rec},3} = 0.969$ for triangular and rectangular lattices, respectively. The poorer fidelity in rectangular lattice is due to the additional population leakage to the auxiliary qubit.

The master-equation simulation of step 2 contains the density matrix of 19 qubits, which is beyond our computer's memory capability. Therefore, we use a Monte Carlo simulation [58,59] which is based on state vector instead of density matrix. Based on the original Hamiltonian of the superconducting qubit lattices, we first simulate the step-1 process using the Monte Carlo approach. Then we take the average output state as the initial state of step 2. The simulated evolution of the GHZ-state fidelity in step 2 is shown in Fig. 5. When the evolution time t in step 2 equals to the controlled-iSWAP gate time $t_{i\mathrm{SWAP}}$, there is a maximum fidelity $F_{\mathrm{tri}}^{(2)} = 0.811$ for a 19-qubit GHZ state in the triangular lattice while $F_{\mathrm{rec}}^{(2)} = 0.804$ for a 13-qubit GHZ state in the rectangular lattice. The GHZ-state fidelity can also be estimated based on the fidelity in the former step. For example, $F_{\mathrm{tri}}^{(2)} \approx F_{\mathrm{tri}}^{(1)} \times \left(F_{\mathrm{tri},3}\right)^6 \times 0.98 = 0.813$, where $\left(F_{\mathrm{tri},3}\right)^6$ accounts for six $U_{\mathrm{MCS},1}$ gates in parallel and 0.98 is due to the decoherence of Q_0 in the gate time with parameters $T_1 = 20\ \mu$s and $T_2^* = 5\ \mu$s. One can see that the estimation agrees well with the Monte Carlo simulation. For the simulation of step 3, the memory requirement goes beyond our computer's memory capability again, even in the Monte Carlo approach. We estimate the 37-qubit GHZ-state fidelity of $F_{\mathrm{tri}}^{(3)} \approx F_{\mathrm{tri}}^{(2)} \times \left(F_{\mathrm{tri},3}\right)^9 \times 0.98^7 = 0.605$ for the triangular lattice, and the 25-qubit GHZ-state fidelity of $F_{\mathrm{rec}}^{(3)} \approx F_{\mathrm{rec}}^{(2)} \times \left(F_{\mathrm{rec},3}\right)^6 \times 0.98^7 = 0.578$ for the rectangular lattice. Both of these two fidelities are higher than the 0.5 threshold for multipartite entanglement [60].

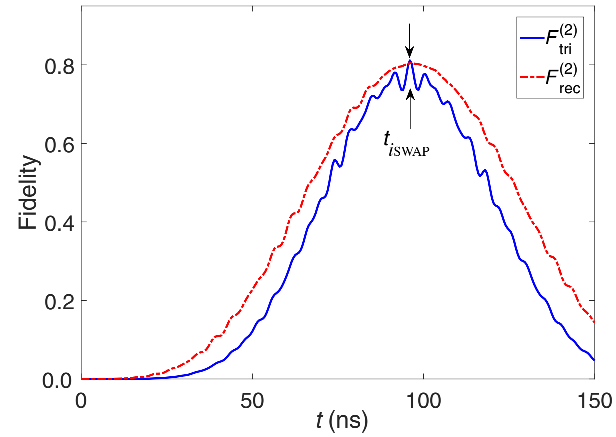

FIG. 5. Time evolution of the 19-qubit (13-qubit) GHZ fidelity $F_{\mathrm{tri}}^{(2)}$ ($F_{\mathrm{rec}}^{(2)}$) in step 2 for triangular (rectangular) lattice. At $t = t_{i\mathrm{SWAP}} = 96$ ns, $F_{\mathrm{tri}}^{(2)}$ ($F_{\mathrm{rec}}^{(2)}$) reaches its maximum value 0.811 (0.804). Relevant parameters are the same as in Fig. 4.

Our proposal does not target a particular type of superconducting qubit, and the implementation of multiqubit controlled-iSWAP gates does not require using an auxiliary level. If the superconducting qubits in the lattices are transmons with weak anharmonicity, it is necessary to consider the influence of higher excited states. For example, when the central qubit Q_0 is in the excited state $|1\rangle$, besides $|0_0 1_1 1_2\rangle$, there is another intermediate state, $|2_0 0_1 0_2\rangle$, for the second-order coupling $|1_0 1_1 0_2\rangle \leftrightarrow |1_0 0_1 1_2\rangle$, where $|2\rangle$ is the second excited state of the transmons. The additional coupling strength is $\lambda' = \left(\sqrt{2}g_1\right)^2 / (\eta - \Delta_1)$, where $\eta = \omega_{10} - \omega_{21}$ is the qubit anharmonicity with ω_{10} (ω_{21}) being the $|1\rangle \leftrightarrow |0\rangle$ ($|2\rangle \leftrightarrow |1\rangle$) transition frequency, and $\sqrt{2}g_1$ is the coupling strength associated with the $|1\rangle \leftrightarrow |2\rangle$

transition. To turn off the $Q_1 - Q_2$ coupling when Q_0 is in the ground state, we still set $g_{12} = \lambda$. Then the total coupling strength is $2\lambda + \lambda'$ when Q_0 is in the excited state $|1\rangle$. Under the condition $\Delta_1 < \eta$, the presence of the second excited state increases the total coupling strength. Therefore, the controlled-*i*SWAP gate time can be shortened, which is beneficial to the gate fidelity.

During the generation of the GHZ states as described above, there are two major error sources: one is the population leakage to the control qubits or the auxiliary qubits; the other is decoherence from qubits. We can reduce the population leakage by selecting appropriate detuning, which makes the high-frequency oscillations nearly return to their initial values at the controlled-*i*SWAP gate time. The decoherence is the biggest obstacle for preparing the GHZ states. As the above simulation results demonstrate, our scheme can generate a GHZ state involving nearly 40 superconducting qubits with T_1 and T_2 available in recent practical experiments.

V. CONCLUSION

We propose a promising mechanism for generating GHZ states, which is especially suitable for 2D superconducting-qubit lattices. An effective three-body interaction, which indicates the energy exchange between two qubits depends on the state of the third qubit, can be easily synthesized on the lattices. Based on the three-body interaction, a multiqubit controlled-*i*SWAP gate can be naturally implemented. We present the protocol to generate GHZ states using the multiqubit controlled-*i*SWAP gate on triangular and rectangular superconducting-qubit lattices. With experimental feasible parameters, our simulation results show that a 37-qubit GHZ state with a fidelity of 0.605 can be generated with a controlled-*i*SWAP depth of 3. Our work provides a promising way to generate larger-scale entangled states on the latest 2D superconducting-qubit architectures with more than 50 qubits.

ACKNOWLEDGMENTS

This work is supported by the National Natural Science Foundation of China (Grants No. 12204139, No. 12205069, No. 11774076, No. U20A2076, and No. U21A20436) and the Key-Area Research and Development Program of GuangDong province (Grant No. 2018B030326001).

[1] John S. Bell, On the Einstein Podolsky Rosen paradox, Physics **1**, 195 (1964).

[2] J. W. Pan, D. Bouwmeester, M. Daniell, H. Weinfurter, and A. Zeilinger, Experimental test of quantum nonlocality in three-photon Greenberger-Horne-Zeilinger entanglement, Nature (London) **403**, 515 (2000).

[3] J. Handsteiner, A. S. Friedman, D. Rauch, J. Gallicchio, B. Liu, H. Hosp, J. Kofler, D. Bricher, M. Fink, C. Leung, Anthony Mark, Hien T. Nguyen, Isabella Sanders, Fabian Steinlechner, Rupert Ursin, Sören Wengerowsky, Alan H. Guth, David I. Kaiser, Thomas Scheidl, and Anton Zeilinger, Cosmic Bell Test: Measurement Settings from Milky Way Stars, Phys. Rev. Lett. **118**, 060401 (2017).

[4] R. Raussendorf and H. J. Briegel, A One-Way Quantum Computer, Phys. Rev. Lett. **86**, 5188 (2001).

[5] M. A. Nielsen and I. L. Chuang, *Quantum Computation and Quantum Information* (Cambridge University Press, Cambridge, 2000).

[6] V. Giovannetti, S. Lloyd, and L. Maccone, Quantum-enhanced measurements: Beating the standard quantum limit, Science **306**, 1330 (2004).

[7] D. M. Greenberger, M. A. Horne, A. Shimony, and A. Zeilinger, Bell's theorem without inequalities, Am. J. Phys. **58**, 1131 (1990).

[8] D. Leibfried, M. D. Barrett, T. Schaetz, J. Britton, J. Chiaverini, W. M. Itano, J. D. Jost, C. Langer, and D. J. Wineland, Toward Heisenberg-limited spectroscopy with multiparticle entangled states, Science **304**, 1476 (2004).

[9] M. Hillery, V. Buzek, and A. Berthiaume, Quantum secret sharing, Phys. Rev. A **59**, 1829 (1999).

[10] A. Zeilinger, M. A. Horne, H. Weinfurter, and M. Żukowski, Three-Particle Entanglements from Two Entangled Pairs, Phys. Rev. Lett. **78**, 3031 (1997).

[11] D. Bouwmeester, J.-W. Pan, M. Daniell, H. Weinfurter, and A. Zeilinger, Observation of Three-Photon Greenberger-Horne-Zeilinger Entanglement, Phys. Rev. Lett. **82**, 1345 (1999).

[12] L. K. Chen, Z. D. Li, X. C. Yao, M. Huang, W. Li, H. Lu, X. Yuan, Y. B. Zhang, X. Jiang, C. Z. Peng, L. Li, N. L. Liu, X. Ma, C. Y. Lu, Y. A. Chen, and J. W. Pan, Observation of ten-photon entanglement using thin BiB_3O_6 crystals, Optica **4**, 77 (2017).

[13] X.-L. Wang, Y.-H. Luo, H.-L. Huang, M.-C. Chen, Z.-E. Su, C. Liu, C. Chen, W. Li, Y.-Q. Fang, X. Jiang, J. Zhang, Li Li, N.-L. Liu, C.-Y. Lu, and J.-W. Pan, 18-Qubit Entanglement with Six Photons' Three Degrees of Freedom, Phys. Rev. Lett. **120**, 260502 (2018).

[14] S. B. Zheng, One-Step Synthesis of Multiatom Greenberger-Horne-Zeilinger States, Phys. Rev. Lett. **87**, 230404 (2001).

[15] A. Omran, H. Levine, A. Keesling, G. Semeghini, T. T.Wang, S. Ebadi, H. Bernien, A. S. Zibrov, H. Pichler, S. Choi, J. Cui, M. Rossignolo, P. Rembold, S. Montangero, T. Calarco, M. Endres, M. Greiner, V. Vuletić, and M. D. Lukin, Generation and manipulation of Schrödinger cat states in Rydberg atom arrays, Science **365**, 570 (2019).

[16] K. Mølmer and A. Sørensen, Multiparticle Entanglement of Hot Trapped Ions, Phys. Rev. Lett. **82**, 1835 (1999).

[17] T. Monz, P. Schindler, J. T. Barreiro, M. Chwalla, D. Nigg, W. A. Coish, M. Harlander, W. Hansel, M. Hennrich, and R. Blatt, 14-Qubit Entanglement: Creation and Coherence, Phys. Rev. Lett. **106**, 130506 (2011).

[18] I. Pogorelov, T. Feldker, C. D. Marciniak, L. Postler, G. Jacob, O. Kriegelsteiner, V. Podlesnic, M. Meth, V. Negnevitsky, M. Stadler, B. Höfer, C. Wächter, K.

Lakhmanskiy, R. Blatt, P. Schindler, and T. Monz, Compact Ion-Trap Quantum Computing Demonstrator, PRX Quantum **2**, 020343 (2021).

[19] K. Helmerson and L. You, Creating Massive Entanglement of Bose-Einstein Condensed Atoms, Phys. Rev. Lett. **87**, 170402 (2001).

[20] L. You, Creating Maximally Entangled Atomic States in a Bose-Einstein Condensate, Phys. Rev. Lett. **90**, 030402 (2003).

[21] P. Neumann, N. Mizuochi, F. Rempp, P. Hemmer, H. Watanabe, S. Yamasaki, V. Jacques, T. Gaebel, F. Jelezko, and J. Wrachtrup, Multipartite entanglement among single spins in diamond, Sciences **320**, 1326 (2008).

[22] X. W. Xu, Y. J. Zhao, and Y. X. Liu, Entangled-state engineering of vibrational modes in a multimembrane optomechanical system, Phys. Rev. A **88**, 022325 (2013).

[23] K. Takeda, A. Noiri, T. Nakajima, J. Yoneda, T. Kobayashi, and S. Tarucha, Quantum tomography of an entangled three-spin state in silicon, Nat. Nanotechnol. **16**, 965 (2021).

[24] J. Q. You and F. Nori, Atomic physics and quantum optics using superconducting circuits, Nature (London) **474**, 589 (2011).

[25] Y. Makhlin, G. Schon, and A. Shnirman, Quantum-state engineering with Josephson-junction devices, Rev. Mod. Phys. **73**, 357 (2001).

[26] J. Clarke and F. K. Wilhelm, Superconducting quantum bits, Nature (London) **453**, 1031 (2008).

[27] J. E. Mooij, T. P. Orlando, L. Levitov, L. Tian, C. H. van der Wal, and S. Lloyd, Josephson persistent-current qubit, Science **285**, 1036 (1999).

[28] M. Feng, Y. P. Zhong, T. Liu, L. L. Yan, W. L. Yang, J. Twamley, and H. Wang, Exploring the quantum critical behaviour in a driven Tavis-Cummings circuit, Nat. Commun. **6**, 7111 (2015).

[29] W. Feng, Y. Li, and S. Y. Zhu, Effect of atomic distribution on cooperative spontaneous emission, Phys. Rev. A, **89**, 013816 (2014).

[30] Y. Chen *et al.*, Qubit Architecture with High Coherence and Fast Tunable Coupling, Phys. Rev. Lett. **113**, 220502 (2014).

[31] P. Mundada, G. Zhang, T. Hazard, and A. Houck, Suppression of Qubit Crosstalk in a Tunable Coupling Superconducting Circuit, Phys. Rev. Appl. **12**, 054023 (2019).

[32] X. Li, T. Cai, H. Yan, Z. Wang, X. Pan, Y. Ma, W. Cai, J. Han, Z. Hua, X. Han, Y. Wu, H. Zhang, H. Wang, Y. Song, L. Duan, and L. Sun, Tunable Coupler for Realizing a Controlled-Phase Gate with Dynamically Decoupled Regime in a Superconducting Circuit, Phys. Rev. Appl. **14**, 024070 (2020).

[33] B. Foxen *et al.*, Demonstrating a Continuous Set of Two-Qubit Gates for Near-Term Quantum Algorithms, Phys. Rev. Lett. **125**, 120504 (2020).

[34] P. Roushan *et al.*, Chiral ground-state currents of interacting photons in a synthetic magnetic field, Nat. Phys. **13**, 146 (2017).

[35] F. Arute *et al.*, Quantum supremacy using a programmable superconducting processor, Nature **574**, 505 (2019).

[36] M. Gong *et al.*, Quantum walks on a programmable two-dimensional 62-qubit superconducting processor, Science **372**, 948 (2021).

[37] Y. Wu *et al.*, Strong Quantum Computational Advantage Using a Superconducting Quantum Processor, Phys. Rev. Lett. **127**, 180501 (2021).

[38] X. Zhang *et al.*, Digital quantum simulation of Floquet symmetry-protected topological phases, Nature **607**, 468 (2022).

[39] W. Ren *et al.*, Experimental quantum adversarial learning with programmable superconducting qubits, arXiv:2204.01738 (2022).

[40] C.-P. Yang and S. Han, Preparation of Greenberger-Horne-Zeilinger entangled states with multiple superconducting quantum-interference device qubits or atoms in cavity QED, Phys. Rev. A **70**, 062323 (2004).

[41] L. F. Wei, Y. X. Liu, and F. Nori, Generation and Control of Greenberger-Horne-Zeilinger Entanglement in Superconducting Circuits, Phys. Rev. Lett. **96**, 246803 (2006).

[42] F. Helmer and F. Marquardt, Measurement-based synthesis of multiqubit entangled states in superconducting cavity QED, Phys. Rev. A **79**, 052328 (2009).

[43] L. S. Bishop, L. Tornberg, D. Price, E. Ginossar, A. Nunnenkamp, A. A. Houck, J. M. Gambetta, J. Koch, G. Johansson, S. M. Girvin, and R. J. Schoelkopf, Proposal for generating and detecting multi-qubit GHZ states in circuit QED, New J. Phys. **11**, 073040 (2009).

[44] Y. D. Wang, S. Chesi, D. Loss, and C. Bruder, One-step multiqubit Greenberger-Horne-Zeilinger state generation in a circuit QED system, Phys. Rev. B **81**, 104524 (2010).

[45] S. Aldana, Y. D. Wang, and C. Bruder, Greenberger-Horne-Zeilinger generation protocol for N superconducting transmon qubits capacitively coupled to a quantum bus, Phys. Rev. B **84**, 134519 (2011).

[46] W. Feng, P. Wang, X. Ding, L. Xu, and X. Q. Li, Generating and stabilizing the Greenberger-Horne-Zeilinger state in circuit QED: Joint measurement, Zeno effect, and feedback, Phys. Rev. A **83**, 042313 (2011).

[47] C.-P. Yang, Preparation of n-qubit Greenberger-Horne-Zeilinger entangled states in cavity QED: An approach with tolerance to nonidentical qubit-cavity coupling constants, Phys. Rev. A **83**, 062302 (2011).

[48] C.-P. Yang, Q.-P. Su, and S. Han, Generation of Greenberger-Horne-Zeilinger entangled states of photons in multiple cavities via a superconducting qutrit or an atom through resonant interaction, Phys. Rev. A **86**, 022329 (2012).

[49] C.-P. Yang, Q.-P. Su, S.-B. Zheng, and S. Han, Generating entanglement between microwave photons and qubits in multiple cavities coupled by a superconducting qutrit, Phys. Rev. A **87**, 022320 (2013).

[50] L. DiCarlo, M. D. Reed, L. Sun, B. R. Johnson, J. M. Chow, J. M. Gambetta, L. Frunzio, S. M. Girvin, M. H. Devoret, and R. J. Schoelkopf, Preparation and measurement of three-qubit entanglement in a superconducting circuit, Nature (London) **467**, 574 (2010).

[51] M. Neeley, R. C. Bialczak, M. Lenander, E. Lucero, M. Mariantoni, A. D. O'Connell, D. Sank, H. Wang, M. Weides, J. Wenner, Y. Yin, T. Yamamoto, A. N. Cleland, and John M. Martinis, Generation of three-qubit entangled states using superconducting phase qubits, Nature (London) **467**, 570 (2010).

[52] R. Barends *et al.*, Superconducting quantum circuits at the surface code threshold for fault tolerance, Nature **508**, 500 (2014).

[53] K. X. Wei, I. Lauer, S. Srinivasan, N. Sundaresan, D. T. McClure, D. Toyli, D. C. McKay, J. M. Gambetta, and S. Sheldon, Verifying multipartite entangled Greenberger-Horne-Zeilinger states via multiple quantum coherences, Phys. Rev. A **101**, 032343 (2020).

[54] C. Song, K. Xu, W. Liu, C.-P. Yang, S.-B. Zheng, H. Deng, Q. Xie, K. Huang, Q. Guo, L. Zhang, P. Zhang, D. Xu, D. Zheng, X. Zhu, H. Wang, Y.-A. Chen, C.-Y. Lu, S. Han, and J.-W. Pan, 10-Qubit Entanglement and Parallel Logic Operations with a Superconducting Circuit, Phys. Rev. Lett. **119**, 180511 (2017).

[55] C. Song, K. Xu, H. Li, Y. Zhang, X. Zhang, W. Liu, Q. Guo, Z. Wang, W. Ren, J. Hao, H. Feng, H. Fan, D. Zheng, D. Wang, H. Wang, and S. Zhu, Generation of multicomponent atomic Schrödinger cat states of up to 20 qubits, Science **365**, 574 (2019).

[56] W. Feng and D. Wang, Quantum Fredkin gate based on synthetic three-body interactions in superconducting circuits, Phys. Rev. A **101**, 062312 (2020).

[57] S. Trotzky, P. Cheinet, S. Fölling, M. Feld, U. Schnorrberger, A. M. Rey, A. Polkovnikov, E. A. Demler, M. D. Lukin, and I. Bloch, Time-resolved observation and control of superexchange interactions with ultracold atoms in optical lattices, Science **319**, 295 (2008).

[58] J. R. Johansson, P. D. Nation, and F. Nori, QuTiP: An open-source Python framework for the dynamics of open quantum systems, Comput. Phys. Commun. **183**, 1760 (2012).

[59] J. R. Johansson, P. D. Nation, and F. Nori, QuTiP 2: A Python framework for the dynamics of open quantum systems, Comput. Phys. Commun. **184**, 1234 (2013).

[60] O. Gühue and G. Tóth, Entanglement detection, Phys. Rep. **474**, 1 (2009).